Energy & Environmental Science

Accepted Manuscript

This is an *Accepted Manuscript*, which has been through the Royal Society of Chemistry peer review process and has been accepted for publication.

Accepted Manuscripts are published online shortly after acceptance, before technical editing, formatting and proof reading. Using this free service, authors can make their results available to the community, in citable form, before we publish the edited article. We will replace this *Accepted Manuscript* with the edited and formatted *Advance Article* as soon as it is available.

You can find more information about *Accepted Manuscripts* in the Information for Authors.

Please note that technical editing may introduce minor changes to the text and/or graphics, which may alter content. The journal's standard Terms & Conditions and the Ethical guidelines still apply. In no event shall the Royal Society of Chemistry be held responsible for any errors or omissions in this *Accepted Manuscript* or any consequences arising from the use of any information it contains.

ROYAL SOCIETY OF CHEMISTRY

www.rsc.org/ees

Structural and Optical Properties of Methylammonium Lead Iodide Across the Tetragonal to Cubic Phase Transition: Implications for Perovskite Solar Cells

Claudio Quarti,[a,b,*] Edoardo Mosconi,[a] James M. Ball,[c] Valerio D'Innocenzo,[c,d] Chen Tao,[c] Sandeep Pathak,[e] Henry J. Snaith,[e] Annamaria Petrozza,[c] Filippo De Angelis[a,*]

[a] Computational Laboratory for Hybrid/Organic Photovoltaics (CLHYO), CNR-ISTM, via Elce di Sotto, I-06123, Perugia, Italy.

[b] Laboratory for Chemistry of Novel Materials, Universitè de Mons, Place du Park, 20, 7000 Mons, Belgium.

[c] Center for Nano Science and Technology @Polimi, Istituto Italiano di Tecnologia, via Giovanni Pascoli 70/3, 20133, Milan, Italy

[d] Dipartimento di Fisica, Politecnico di Milano, Piazza L. da Vinci, 32, 20133 Milano, Italy.

[e] University of Oxford, Clarendon Laboratory, Parks Road, Oxford, OX1 3PU, United Kingdom.

E-mail: Claudio.QUARTI@umons.ac.be; filippo@thch.unipg.it

Energy & Environmental Science Accepted Manuscript

Abstract

We report temperature resolved UV-vis absorption and external quantum efficiency measurements of $MAPbI_3$ thin films and solar cells, together with ab-initio simulations, to investigate the changes in material properties occurring across the tetragonal to cubic phase transition. We find that the $MAPbI_3$ band-gap of does not abruptly change when exceeding the tetragonal to cubic transition temperature, but it rather monotonically blue-shifts following the same temperature evolution observed within the tetragonal phase. Car-Parrinello molecular dynamics simulations demonstrate that the high temperature phase corresponds on average to the expected symmetric cubic structure assigned from XRD measurements, but that the system strongly deviates from such a structure in the sub-picosecond time scale. Thus, on the time scale of electronic transitions, the material seldom experiences a cubic environment, rather an increasingly distorted tetragonal one. This result explains the absence of dramatic changes in the optical and photovoltaic properties of $MAPbI_3$ across the explored temperature range of 270-420 K, which could have important consequences for the practical uptake of perovskite solar cells.

Broader context

The rapid efficiency surge of solar cells based on organohalide lead perovskite has been only in part paralleled by a fundamental understanding of the basic materials properties. The prototypical methylammonium lead iodide perovskite, $MAPbI_3$, shows the presence of various phase transitions occurring in the temperature range of technologically relevant applications. Above 327 K, a change from a tetragonal to a cubic structure is known to occur. The presence of such a tetragonal- cubic transition well within the operative temperature range of a solar cell is a delicate point for the widespread uptake of perovskite solar cells, as it could inherently hinder the real word applications of these devices. Here we demonstrate that the photovoltaic properties of hybrid lead-halide perovskites are not inherently limited by the presence of a phase transition within the solar cell operating regime. In particular, we show the absence of dramatic changes in the optical and

Energy & Environmental Science Accepted Manuscript

photovoltaic properties of $MAPbI_3$ perovskites across the tetragonal to cubic transition, due to structural fluctuations on a sub-picosecond timescale that make the instantaneous electronic energy levels and band-gap of the formally cubic, high temperature structure, to differ only slightly from those of the room temperature stable tetragonal phase.

Energy & Environmental Science Accepted Manuscript

1. Introduction.

Hybrid metal halide perovskites of the type $AMX_{3-x}Y_x$, with A= Cesium (Cs), methylammonium (MA) or formamidinium (FA), M=Sn or Pb, and X, Y= Cl, Br and I, represent one of the most important recent breakthroughs in the field of photovoltaics and optoelectronics in general. Initially investigated in dye-sensitized solar cells,[1] showing an impressive efficiency improvement in just a few years,[2-8] with recently reported record efficiency of ~20%,[9] hybrid lead halide perovskites have been successfully implemented also in a variety of optoelectronic applications, such as light emitting devices,[10] lasing[11] and water-splitting devices.[12, 13] Their success is mainly due to their unique set of electronic properties, such as ambipolar transport properties,[14, 15] μm to mm charge carrier diffusion length,[16, 17] low intrinsic recombination rate,[18] tunable band gap across the visible region (down to 1.2 eV for the $MASnI_3$ perovskite),[19] and large absorption coefficient.[2] Notably, these impressive electronic properties are coupled to the possibility to resort to low cost solution-based techniques for their synthesis and deposition, or alternatively to vapor deposition methods,[5] which has further increased the scope for device applications.

In spite of the large body of work, however, there are still many open questions on the basic electro-optical properties of this class of materials and on their possible practical limitations. An important peculiarity that hybrid perovskites share with their fully inorganic counterpart is the presence of various phase transitions, also occurring in the temperature range of technologically relevant applications. An example is provided by the prototypical methylammonium lead iodide perovskite, here-on $MAPbI_3$. X-ray diffraction (XRD) investigations[19, 20] and calorimetric measurements[21, 22] highlighted the presence of two phase transitions at 162 K and at 327 K. Poglitsch and Weber assigned the low temperature transition to a change from an orthorhombic-to-tetragonal crystalline structure, and the high temperature one to a change from a tetragonal-to-cubic structure.[20] The presence of a tetragonal-to-cubic transition at 327 K, well within the operative temperature range of a solar cell, is a delicate point as it could inherently hinder the real word applications of these devices, because of possible variations across the phase transition of the

Energy & Environmental Science Accepted Manuscript

inherent optoelectronic properties of this class of materials and consequently of its photovoltaic working mechanism.

This point has been partly addressed by a recent paper by Zhang et. al.,[23] who investigated the photovoltaic performances of $MAPbI_3$ in the 80 K to 360 K temperature range, thus across both the orthorhombic-tetragonal and the tetragonal-cubic phase transitions. These authors demonstrated that the photovoltaic parameters of $MAPbI_3$-based solar cells, especially short circuit current and fill factor, did not change dramatically across the tetragonal-cubic phase transition at 327 K, while they observed a strong efficiency decrease when approaching the orthorhombic phase. These results seem to suggest that there could be no marked distinction between the tetragonal and cubic phases, while the orthorhombic phase shows effectively different photovoltaic properties. An important point to be further explored is whether the fundamental material properties affecting the photovoltaic operational mechanism in perovskite solar cells, i.e. the perovskite band-gap and energy levels, are changing across the tetragonal-cubic phase transition and to what extent. This information is fundamental for the device design, since a significant change in the perovskite electronic structure typically associated with a phase transition is difficult to accommodate in a device whilst maintaining efficient charge extraction with carrier-selective contacts as they must be well matched to the light-absorber over all conditions.

In this paper, we present a coupled experimental and theoretical investigation aimed at clarifying, at an atomistic level, the variation of the structural and optical properties of $MAPbI_3$ across the tetragonal-cubic phase transition. We perform UV-vis absorption and external-quantum-efficiency (EQE) measurements as a function of temperature both on $MAPbI_3$ and on $MAPbI_{3-x}Cl_x$ perovskites in the 300-410 K range, comparing with previous results at lower temperatures.[24] We observe a gradual blue-shift of the band-gap from room temperature to 410 K, that is not paralleled by the predictions of GW calculations for an abrupt change from the tetragonal to the cubic structure. Car-Parrinello molecular dynamics simulations reveal that the high temperature phase is indeed cubic when considering the time-averaged structure. However, we observe large fluctuations

Energy & Environmental Science Accepted Manuscript

in the PbI_6 octahedra tilting on a sub-picosecond timescale *that make the instantaneous and time-averaged band-gap distinctively wider than the band-gap predicted for the time-averaged structure*, consistent with our experimental evidence. This result explains the absence of dramatic changes in the optical and photovoltaic properties of $MAPbI_3$ perovskites across the explored temperature range. Most notably, we demonstrate that, as opposed to the ferroelectric properties of inorganic oxide perovskites, the photovoltaic properties of hybrid lead-halide perovskites are not inherently limited by the presence of a phase transition within the solar cell operating regime.

2. Results and Discussion.

The transition from the room temperature tetragonal phase to the high temperature cubic phase of hybrid lead-halide perovskites has been widely studied in the past. Calorimetric studies by Knop et. al.[22] and by Onoda-Yamamuro et. al.[21] reported large latent heat during this transition, demonstrating that it is a first-order thermodynamic transition. On the structural side, the tetragonal-cubic transition in $MAPbBr_3$ and $MAPbI_3$ has been classified by Mashiyama et. al. as displacive.[25] The typical "out-of-phase" rotation of the PbI_6 octahedra along the *c*-axis of the tetragonal phase, $a^0a^0c^-$ structure in the Glazer notation,[26] gradually reduces when increasing the temperature, until the octahedra are no longer rotated, on average, thus resulting in a cubic structure classified as $a^0a^0a^0$, see Figure 1. The rotation of the octahedra can be quantified by the I-Pb-Pb-I dihedral angle, α in Figure 1. The gradual reduction of the octahedra tilting in $MAPbI_3$ is supported by recent XRD analyses.[27, 28]

Energy & Environmental Science Accepted Manuscript

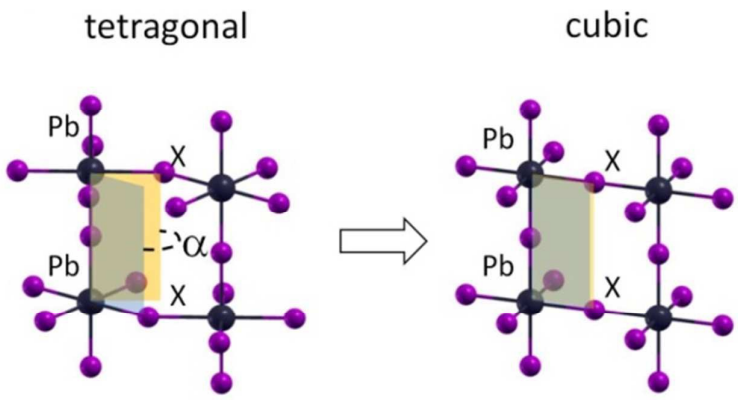

Figure 1. Octahedra tilting pattern for the tetragonal (left) to the cubic (right) structure of in a $MAPbX_3$ perovskite (X=halide); the order parameter of the transition, the X-Pb-Pb-X dihedral angle α, is also reported.

In Figure 2a, we report the UV-vis absorption spectrum of $MAPbI_3$ from 310 K to 400 K . Data recorded in the full 4.2-400 K temperature range can be found in Supplementary Information. Within the temperature stability range of the tetragonal phase, we observe a gradual blue-shift of the absorption maximum with increasing temperature from ~1.61 to ~1.69 eV (Figure 2a). For many semiconductors (Si, Ge, GaAs, InP, InAs…) the band gap red-shifts to lower energies with increasing temperature. Some Pb-based compounds instead show the opposite results. In PbS films for example, lattice dilation increases the band gap.[30] A similar result has been theoretically reported for $MAPbI_3$.[29, 31] We fitted this shift with a linear approximation of the empirical Varshni relationship[32] in the high temperature limit, also considering that the absence of an excitonic transition allows for a clear linear fit of the change in the band gap onset as a function of the temperature according to equation 1:

$$E_g(T)=E_g(0)+dE_g/dT*T \quad (1)$$

where $E_g(0)$ represents the material energy gap at T=0, while dE_g/dT is a constant parameter characteristic of a given material which has contributions from lattice thermal expansion and electron-phonon interactions.[32] The fitting provides an estimate of the temperature dependence of

Energy & Environmental Science Accepted Manuscript

the band gap of $dE_g/dT=257\pm13$ μeV/K for $MAPbI_3$ (Figure 2b). A recent work, confirms this continuous blue-shift of the band gap across the tetragonal-cubic transition for $MAPbI_3$, and it demonstrates that this is mainly due to the down-shift of the valence band.[33] For $MAPbI_{3-x}Cl_x$ our measured absorption spectra show a similar behavior as for $MAPbI_3$ but suggest a ~20 K lower orthorhombic to tetragonal transition temperature for this material, Supplementary Information Figure S1, in line with the effect of a small percentage of chlorine doping.[40]

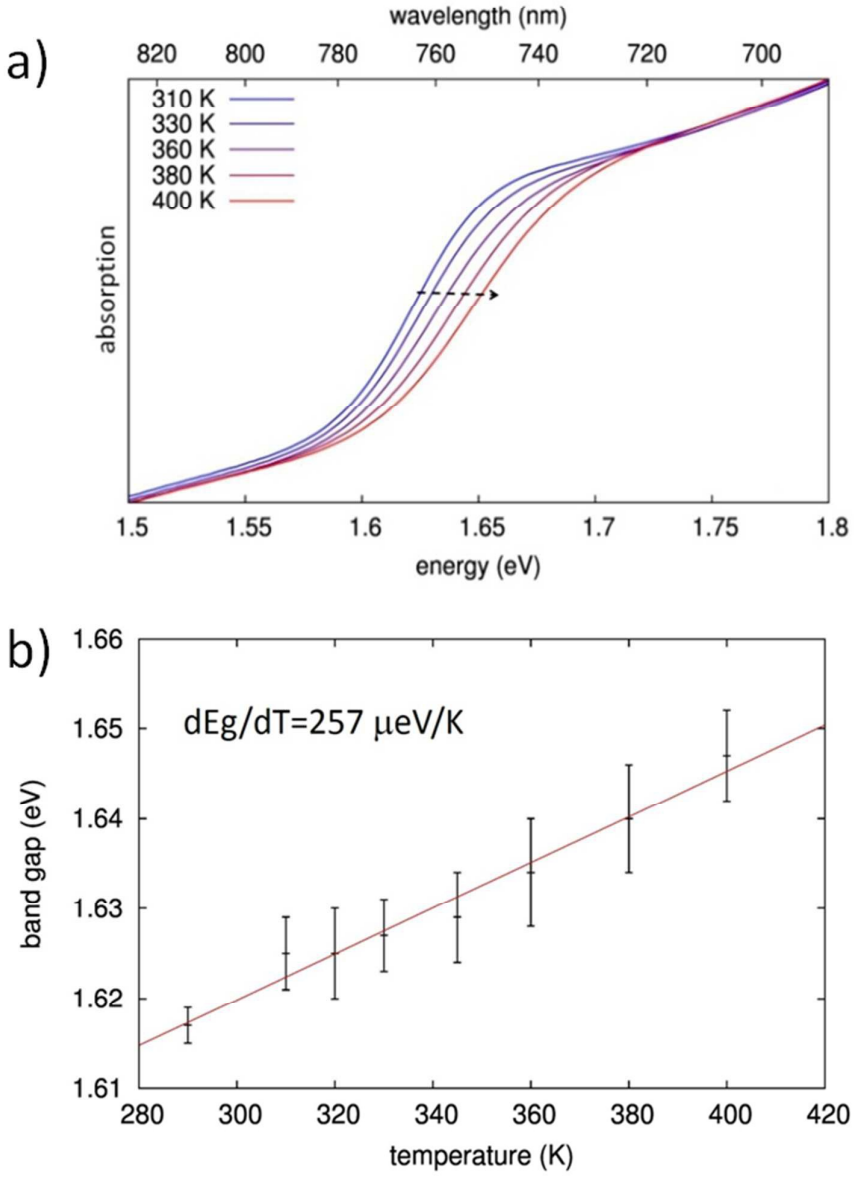

Energy & Environmental Science Accepted Manuscript

Figure 2. a) UV-vis absorption spectrum of of $MAPbI_3$ from 310 K to 400 K; b) evolution of the band gap The experimental data are fitted according to equation (eq.1) to extrapolate dEg/dT=257 ±13 μeV/K.

Most notably, our observations are directly translated into the photovoltaic properties of devices based on $MAPbI_3$, fabricated according to recently published procedure.[34] In Figure 3a-b, we report the J-V curve and absolute external quantum efficiency (EQE) of a 17.4% efficient solar cell (see Experimental Methods, Supplementary Information, for further details). In Figure 3c we report the normalized EQE for the same cell scanned across the 300-360 temperature range. The cell was first heated from 300 K to 360 K, above the tetragonal-cubic transition, then cooled down back to 300 K to verify the reversibility of the spectral shift and the absence of permanent changes in the light-harvesting spectrum induced by thermal cycling in $MAPbI_3$-based solar cells. Heating from 300 K to 360 K, we observe a gradual blue-shift of the EQE curve onset, that is related to the increase of the band gap of Figure 2a, consistent with changes in the absorption spectrum of bare $MAPbI_3$ films. Interestingly, we do not observe abrupt variations of the spectral dependence of the photocurrent generation across the tetragonal-cubic phase transition, consistent with the similar short circuit current and efficiencies found by Zhang et. al.-.[23] Cooling down from 360 K to 300 K, we observe a complete recovery of the original spectral shape of the EQE, thus demonstrating that the variation in band-gap across the tetragonal-cubic phase transition is completely reversible in an efficient functioning device. We repeated the measurements for several $MAPbI_3$-based devices with power conversion efficiencies >15 % (Figure SI2 and SI3) to ensure the reproducibility of the phenomena A similar trend was also observed in a $MAPbI_{3-x}Cl_x$–based device (Figure SI4).

Energy & Environmental Science Accepted Manuscript

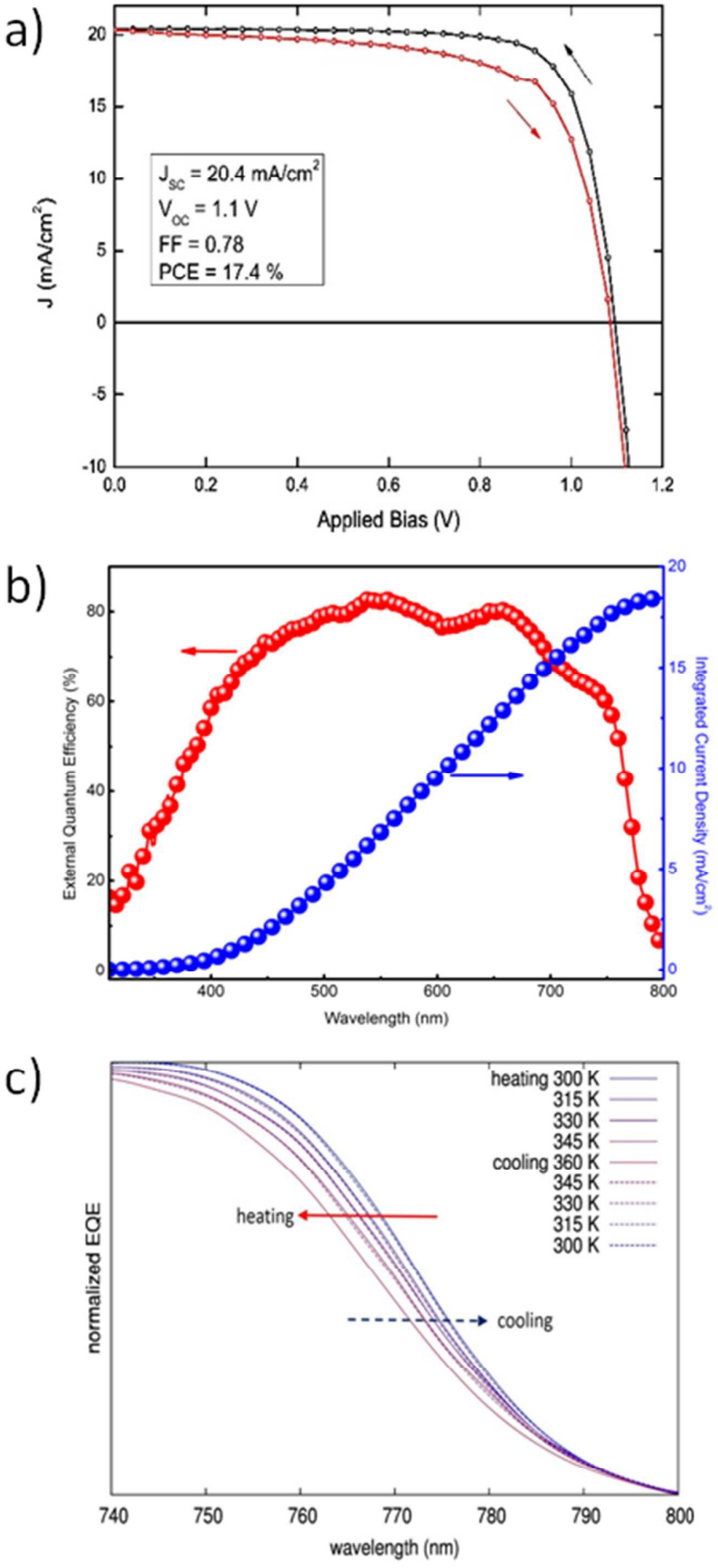

Energy & Environmental Science Accepted Manuscript

Figure 3. a) J-V curve and b) absolute EQE for a $MAPbI_3$-based solar cell at room temperature. c) Normalized EQE for the same photovoltaic device across the temperature range of the tetragonal-cubic phase transition.

To provide a rationale for the picture derived from experimental measurements, we performed periodic quantum-mechanical calculations, using the Quantum-Espresso suite of programs.[35] First, we calculated the electronic band gap of the orthorhombic, tetragonal and cubic crystals at their optimized geometry. To provide reliable bang-gap estimates, we resorted to state-of-art GW calculations with the inclusion of spin-orbit-coupling (SOC), currently representing the method of choice for accurate predictions, within 0.1 eV, of the electronic properties of hybrid lead halide perovskites.[36, 37] In light of the very small chlorine concentration in $MAPbI_{3-x}Cl_x$, around a few % at most,[38-41] we limited our simulations to the pristine $MAPbI_3$ perovskite. For the orthorhombic phase, we used the P_{nma} structure determined from the XRD measurements at 100 K by Baikie et al.,[27] made by four $MAPbI_3$ units. For the tetragonal phase we used a previously optimized structure,[42, 43] again made by four $MAPbI_3$ units, which is consistent with the XRD structures proposed by Kawamura et. al.[44] and Stoumpos et. al.,[19] showing the typical $a^0a^0c^-$ rotation of the PbI_6 octahedral, Figure 1a. For the cubic structure, our model is made by eight $MAPbI_3$ units obtained by replication of two different optimized cubic systems made by one $MAPbI_3$ unit. The two structures are originated by fixing the inorganic atoms in the crystallographic cubic positions and by relaxed the organic MA cation, hereafter (a), or by allowing the organic and inorganic components to relax (b). In all cases, we used the experimental cell parameters (see Supplementary Information for further details).[20]

Table 1. Comparison between experimental band-gap (eV) of the various phases of $MAPbI_{3-x}Cl_x$, and the calculated SOC-GW band gap of $MAPbI_3$. (a) and (b) refer to the two considered cubic structures, see text for definitions. In parenthesis, we report the temperature at which the

Energy & Environmental Science Accepted Manuscript

experimental band gap is evaluated.

	orthorhombic	tetragonal	cubic
exp.	1.65 (4.2 K)	1.61 (160 K)	1.69 (330 K)
SOC-GW	1.81	1.67	1.16[(a)]/1.28[(b)]

The SOC-GW band-gap calculated for the three phases of $MAPbI_3$ at their optimized structures are reported in Table 1, compared with experimental data from Figure 2 and Figure SI1. We predict a red-shift associated to the orthorhombic-to-tetragonal change in the crystal structure, from 1.81 eV to 1.67 eV, in good agreement with the red-shift from 1.65 eV to 1.61 eV observed from the UV-vis measurements, Figure SI1. Notice that while for the orthorhombic phase an excitonic feature is clearly visible in the optical spectra, no such feature is distinguishable for the tetragonal phase. Thus for the orthorhombic phase the optical absorption maximum represents a lower-bound for the electronic band-gap, which is the SOC-GW calculated quantity, while the two values may coincide (within few meV) for the tetragonal phase. Our SOC-GW calculated band-gap for the orthorhombic phase agrees with previous data obtained for this system by hybrid functionals including SOC.[32] For the high temperature transition instead, SOC-GW calculations predict a large red-shift of the band-gap, amounting to 0.4-0.5 eV, that is clearly inconsistent with the experimental data in Figure 2.

These results demonstrate that, in spite of the expected reliability of SOC-GW calculations, a static picture based on the optimized structures is not able to explain the experimental data for the tetragonal-cubic phase transition. In this sense, several results reported in the literature have questioned the presence of a highly symmetric cubic crystal structure in the high temperature phase of methylammonioum lead halide perovskites. XRD studies by Mashiyama et. al. pointed out that the Cl anions do not occupy exactly the cubic symmetry positions in the high temperature of $MAPbCl_3$;[45] Worhatch et. al observed large rotations of the $PbBr_6$ octahedra, for the high

Energy & Environmental Science Accepted Manuscript

temperature cubic phase of $MAPbBr_3$, with the local material structure that can differ from the nominal $a^0a^0a^0$ structure of Figure 1a;[46] Abid et. al. observed a signal at 66 cm^{-1} in the Raman spectrum of the high temperature phase of $MAPbCl_3$, that, due to symmetry reasons, should be silent.[47] Hybrid lead halide perovskites are well known to show important structural dynamics phenomena at room temperature, in particular in relation to the rotational motion of the MA cations within the perovskite cubo-octahedral cavity.[20, 21, 48] To account for these effects on the material structure and consequently on the electronic properties, we performed Car-Parrinello molecular dynamics (CPMD)[49] simulations on models representative of the room temperature tetragonal phase and of the high temperature cubic phase. For both the tetragonal and cubic phases, we employed a 2x2x2 replica of the tetragonal crystallographic cell containing 4 $MAPbI_3$ units (thus a 32 $MAPbI_3$ system is simulated), using the experimental cell parameters reported by Poglitsch and Weber.[20] The employed 2x2x2 model cell, containing 384 atoms, provides reliable results for the structural properties of the $MAPbI_3$ perovskite,[43, 50] as inferred by comparing the radial distribution function obtained from the theory to the experimental data[51] (Figure SI5). The tetragonal phase is simulated at an average temperature of 320 K, using the real atomic masses for all the atoms, except hydrogen which is replaced by deuterium, for a total time simulation of 18 ps, after a few ps of equilibration. The cubic phase is simulated starting from the same structure at an average temperature of 650 K and the total simulation time for the cubic structure is limited to 6 ps, after few ps of equilibration (for further details see Supplementary Information). First, we analyzed the averaged crystalline structure within the duration of the simulation. The time-averaged structures observed during the CPMD simulation are shown in Figure 4a-b, respectively, for the 320 K and the 650 K simulations. For the simulation at 320 K, we observe the "out-of-phase" rotation of the PbI_6 octahedra rotation along the *c*-axis (see Figure 4a), typical of the tetragonal structure of $MAPbI_3$.[19, 44] For the simulation at 650 K instead, the time-averaged structure is essentially cubic, with only a small residual octahedra tilting, reasonably due to the constraint on the cell parameters, that were fixed to the experimental parameters of the tetragonal phase and are thus shorter with respect to the

Energy & Environmental Science Accepted Manuscript

equilibrium cell parameters of the cubic phase. Thus, the 320 K structure and the 650 K on the ps time scale actually correspond to the nominal $a^0a^0c^-$ and $a^0a^0a^0$ structures experimentally evinced from XRD measurements. The statistical analysis of the dihedral I-Pb-Pb-I angles confirms this result (see Figure 4c-d). The 320 K structure shows a nearly symmetric distribution typical of the $a^0a^0c^-$ tetragonal phase, with α maximum values at ±28°. The 650 K structure instead presents a nearly symmetric distribution centered around an α value of 0°. Most notably, the "cubic" structure can strongly deviate from the nominal $a^0a^0a^0$ structure on a sub-ps time scale, with octahedra tilting values comparable to those observed for the tetragonal 320 K structure. Noteworthy, the probability for a dihedral I-Pb-Pb-I angle in the high temperature phase of being larger or smaller than ±10° is as much as 50%. Thus, locally and on a sub-ps time-scale, the structure is on average significantly distorted with respect to the nominally cubic $a^0a^0a^0$ symmetry.

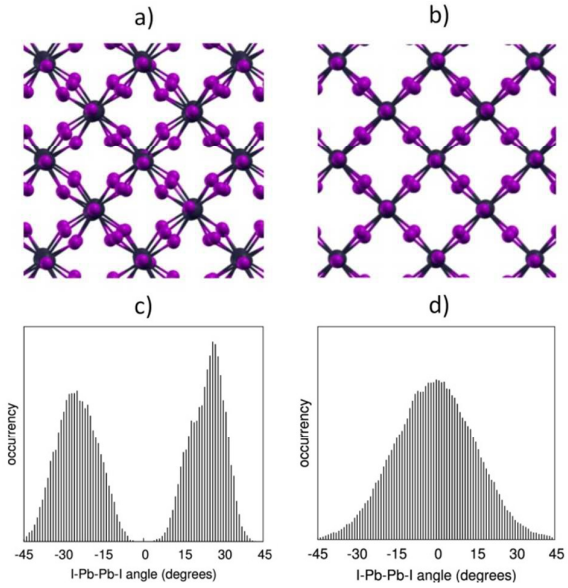

Figure 4. a) and b) Structure for the 320 K and 650 K, averaged over the whole CPMD simulation time. c) and d) distribution of the values assumed by all the I-Pb-Pb-I dihedral angles within the periodic cells, during the CPMD simulation, respectively for the 320 K simulation (c) and for the 650 K (d). For a definition of the I-Pb-Pb-I dihedral angles, see Figure 1a.

Energy & Environmental Science Accepted Manuscript

Now, we investigate the effect of these sub-ps dynamical fluctuations on the electronic properties of $MAPbI_3$. First, we calculate the scalar-relativistic (SR) DFT and the SOC-DFT band-gap of the time-averaged structures. This is accomplished by averaging the atomic positions during the CPMD dynamics at each temperature, leading to two structures (one for the high T and one for the low T) which are reported in Figure 4a-b. As previously discussed, SR-DFT fortuitously reproduces the experimental band gap value and that found by more elaborate SOC-GW calculations,[36, 42] while SOC-DFT considerably underestimates the band gap[52] but it still provides qualitatively similar results to SOC-GW calculations.[53] The results are reported in Table 2. The small SOC-DFT band gap obtained for the time-averaged high temperature structure compares well with the data from Ref. [37] (0.2 eV) and Ref. [53] (0.16 eV). Similarly, for the low temperature time-averaged structure the calculated band-gap is consistent with previous data. We then computed the instantaneous band-gap fluctuations at 320 K and 650 K by explicitly calculating the band-gap of each structure encountered during the structural dynamics, thus considering inherently the effects of the structural deformations on the electronic properties of $MAPbI_3$, see Figure 5 and Supplementary Information. For the dynamics at 320 K, the band-gap oscillates around an average value of 1.62/0.59 eV (SR-DFT/SOC-DFT), thus only slightly increasing with respect to the 1.50/0.40 eV (SR-DFT/SOC-DFT) band-gap computed on the time-averaged structure. At 650 K, the band gap oscillates around 1.67/0.77 eV (SR-DFT/SOC-DFT), being significantly larger than the band gap calculated on the time-averaged structure, 1.24/0.04 eV by SR-DFT/SOC-DFT. Most notably, a blue-shift of the band-gap across the tetragonal-cubic structure is observed, from 1.62 eV to 1.67 eV at the SR-DFT level (from 0.59 eV to 0.77 eV at the SOC-DFT level), that agrees quite well with the experimentally observed blue-shift, Table 2. As mentioned above, the present CPMD simulations do not consider the inherent variation of the crystalline cell parameters with the temperature,[33] but still they partly recover than observed band-gap variation, pointing at the dynamics of the PbI_6 octahedra rotation across the phase transition as a source of band-gap increase with increasing temperature.

Energy & Environmental Science Accepted Manuscript

Table 2. Theoretical band gap calculated on i) the time-average structure from CPMD simulations and ii) as the average of the band gap during the CPMD simulations. Band-gaps are evaluated both at the scalar-relativistic (SR-DFT) and at the spin-orbit-coupling (SOC-DFT) level of theory.

	SR-DFT	SOC-DFT
T (K)	band-gap of the time-averaged structure	
320	1.50	0.40
650	1.24	0.04
T (K)	average of the instantaneous band-gap	
320	1.62	0.59
650	1.67	0.77

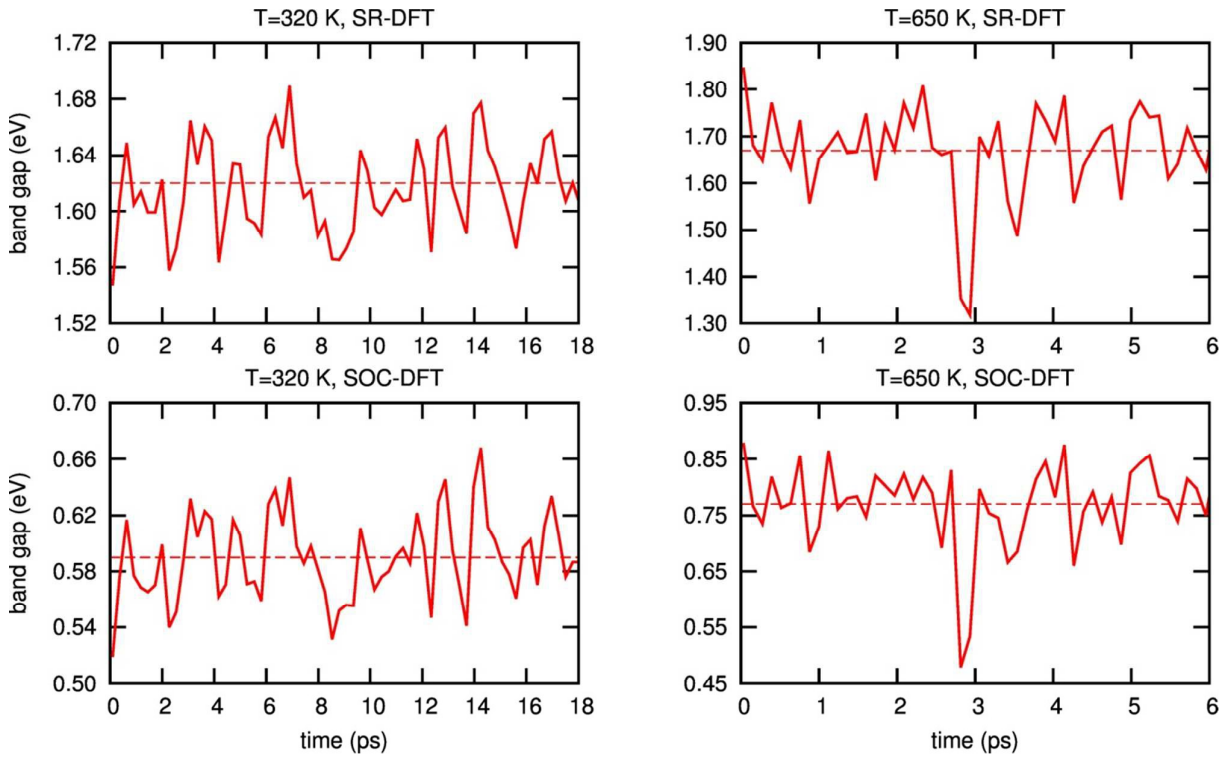

Figure 5. Evolution of the band gap during the CPMD simulations for the system at 320 K and at 650 K, evaluated at the SR-DFT and SOC-DFT level of theory. The dashed line represents the band-gap average.

Energy & Environmental Science Accepted Manuscript

Our data clearly highlight the presence of large fluctuations in the PbI_6 octahedra tilting on a sub-picosecond timescale that make the instantaneous band-gap and its average value to be distinctively wider than the band-gap predicted for the time-averaged structure, consistent with the experimental evidence. The time evolution of the valence and conduction band edges, whose difference determines the band-gap, seems to be relatively uncorrelated, see Figure SI5, Supplementary Information. Notably, the valence band edge shows larger fluctuations around its average value, in line with the results of Ref. 33 pointing at a variation of the valence band as an additional source of band-gap increase.

3. Conclusions.

In summary, we have reported a combined experimental and theoretical investigation aimed at unraveling the possible electronic structure changes occurring for pristine $MAPbI_3$ and chlorine doped $MAPbI_{3-x}Cl_x$ perovskites across the tetragonal-cubic phase transition. Via temperature-resolved UV-vis absorption of bare films and external-quantum-efficiency measurements in efficient solar cells, we have demonstrated that the band-gap does not show sharp variations across the tetragonal-cubic phase transition. We have also shown by *ab-initio* molecular dynamics simulations that, within ~10 ps time-scale, the material structure agrees very well with the tetragonal and cubic symmetry assigned from X-ray diffraction measurements,[19, 20, 44] while on a sub-picosecond time-scale, typical of the electronic processes probed by UV-vis spectroscopy, we observe that the high temperature phase is strongly distorted with respect to the cubic symmetry. When these instantaneous deviations from the nominal cubic crystalline structure are considered, the blue-shift of the band-gap observed experimentally is correctly reproduced by simulations. This large structural flexibility in the high temperature phase, not only related to the motions of the organic cations but also to fluctuations of the inorganic framework, may explain some literature results that criticized the presence of a rigorously cubic structure in the high temperature phase, as the presence of residual octahedral rotations in the high temperature phase of $MAPbBr_3$,[46] the

Energy & Environmental Science Accepted Manuscript

disordered position of the Cl anions[45] and the presence of a Raman signal at 66 cm^{-1} in the high temperature phase of $MAPbCl_3$.[47] From a technological perspective, these results help to explain the lack of an observable abrupt change in photovoltaic device performance above room temperature[23] as would be expected to be observable if the light-harvester undergoes a phase transition. This is also further evidence indicating that ferroelectricity contributions to the optoelectronic properties, as in traditional inorganic materials,[54-57] are negligible, since the ferroelectric polarizability is expected to change dramatically across the transition between two different crystalline structures. On the contrary, this view supports other proposed mechanisms, as the spatial charge localization[50, 58] and/or stable band bending effects at the interfaces and grain boundaries,[59] as the basis of the impressive inherent performance of hybrid lead halide perovskites.

ASSOCIATED CONTENT

Supplementary Information

Experimental methods; theoretical methods and models; EQE measurements on different MAPbI3 devices; corresponding JV measurements of the devices; EQE of a cell with $MAPbI_{3-xClx}$; comparison between theoretical and experimental radial distribution function of $MAPbI_3$ perovskite; theoretical fluctuation of the band edges.

AUTHOR INFORMATIONS

Corresponding authors:

Claudio Quarti; Filippo De Angelis

ACKNOWLEDGMENT

The research leading to these results has received funds from the European Union Seventh Framework Programme [FP7/2007%2013] under Grant Agreement No. 604032 of the MESO project.

Energy & Environmental Science Accepted Manuscript

References:

1. Kojima, A., K. Teshima, Y. Shirai, and T. Miyasaka, Organometal Halide Perovskites as Visible-Light Sensitizers for Photovoltaic Cells. *J. Am. Chem. Soc.*, 2009. **131**, 6050–6051.
2. Im, J.-H., C.-R. Lee, J.-W. Lee, S.-W. Park, and N.-G. Park, 6.5% Efficient Perovskite Quantum-Dot-Sensitized Solar Cell. *Nanoscale*, 2011. **3**, 4088–4093.
3. Lee, M.M., J. Teuscher, T. Miyasaka, T.N. Murakami, and H.J. Snaith, Efficient Hybrid Solar Cells Based on Meso-Superstructured Organometal Halide Perovskites. *Science*, 2012. **338**, 463-467.
4. Burschka, J., N. Pellet, S.-J. Moon, R. Humphry-Baker, P. Gao, M.K. Nazeeruddin, and M. Graetzel, Sequential Deposition as a Route to High-Performance Perovskite-Sensitized Solar Cells. *Nature*, 2013. **499**, 316-319.
5. Liu, M., M.B. Johnston, and H.J. Snaith, Efficient Planar Heterojunction Perovskite Solar Cells by Vapour Deposition. *Nature*, 2013. **501**, 395-398.
6. Edri, E., S. Kirmayer, D. Cahen, and G. Hodes, High Open-Circuit Voltage Solar Cells Based on Organic−Inorganic Lead Bromide Perovskite. *J. Phys. Chem. Lett.*, 2013. **4**, 897−902.
7. Ball, J.M., M.M. Lee, A. Hey, and H.J. Snaith, Low-temperature processed meso-superstructured to thin-film perovskite solar cells. *Energy Environmental Science*, 2013. **6**, 1739-1743.
8. Malinkiewicz, O., A. Yella, Y.H. Lee, G.M. Espallargas, M. Graetzel, M.K. Nazeeruddin, and H.J. Bolink, Perovskite solar cells employing organic charge-transport layers. *Nature Photonics*, 2014. **8**, 128-132.
9. Zhou, H., Q. Chen, G. Li, S. Luo, T.-B. Song, H.-S. Duan, Z. Hong, J. You, Y. Liu, and Y. Yang, Interface engineering of highly efficient perovskite solar cells. *Science*, 2014. **345**, 542-546.
10. Stranks, S.D. and H.J. Snaith, Metal-halkide perovskites for photovoltaic and light-emitting devices. *Nature Nanotechnology*, 2015. **10**, 391-402.
11. Zhu, H., Y. Fu, F. Meng, X. Wu, G. Zizhou, Q. Ding, M.V. Gustafsson, M.T. Trinh, S. Jin, and X.-Y. Zhu, Lead halide perovskite nanowire lasers with low lasing threshold and high quality factors. *Nature Materials*, 2015. **14**, 636-643.
12. Luo, J., J.-H. Im, M.T. Mayer, M. Schreier, M.K. Nazeeruddin, N.-G. Park, S. David Tilley, H.J. Fan, and M. Gratzel, Water photolysis at 12.3% efficiency via perovskite photovoltaics and earth-abundant catalysts. *Science*, 2014. **345**, 1593-1596.
13. Chen, Y.-S., J.S. Manser, and P.V. Kamat, All solution-processed lead halide perovskite-$BiVO_4$ tandem assembly for photolytic solar fuels production. *Journal of American Chemical Society*, 2015. **137**, 974-981.
14. Edri, E., S. Kirmayer, S. Mukhopadhyay, K. Gartsman, G. Hodes, and D. Cahen, Elucidating the charge charrier separation and working mechanism of $CH_3NH_3PbI_{3-x}Cl_x$ perovskite solar cells. *Nature Communications*, 2014. **5**, 3461/1-8.
15. Edri, E., S. Kirmayer, A. Henning, S. Mukhopadhyay, K. Gartsman, Y. Rosenwaks, G. Hodes, and D. Cahen, Why lead methylammonium tri-iodide perovskite-based colar cells require a mesoporous electron transporting scaffold (but not necessarily a hole conductor). *Nano Letters*, 2014. **14**, 1000-1004.
16. Stranks, S.D., G.E. Eperon, G. Grancini, C. Menelaou, M.J.P. Alcocer, T. Leijtens, L.M. Herz, A. Petrozza, and H.J. Snaith, Electron-Hole Diffusion Lengths Exceeding 1 Micrometer in an Organometal Trihalide Perovskite Absorber. *Science*, 2013. **234**, 341-344.

Energy & Environmental Science Accepted Manuscript

17. Xing, G., N. Mathews, S. Sun, S.S. Lim, Y.M. Lam, M. Graetzel, S. Mhaisalkar, and T.C. Sum, Long-Range Balanced Electronand Hole-Transport Lengths in Organic-Inorganic $CH_3NH_3PbI_3$. *Science*, 2013. **342**, 344-347.
18. Wehrenfennig, C., G.E. Eperon, M.B. Johnston, H.J. Snaith, and L.M. Herz, High Charge Carrier Mobilities and Lifetimes in Organolead Trihalide Perovskites. *Advanced Materials*, 2014. **26**, 1584–1589.
19. Stoumpos, C.C., C.D. Malliakas, and M.G. Kanatzidis, Semiconducting Tin and Lead Iodide Perovskites with Organic Cations: Phase Transitions, High Mobilities, and Near-Infrared Photoluminescent Properties. *Inorg. Chem.*, 2013. **52**, 9019−9038.
20. Poglitsch, A. and D. Weber, Dynamic Disorder in Methylammoniumtrihalogenoplumbates (II) Observed by Millimeterwave Spectroscopy. *J. Chem. Phys.*, 1987. **87**, 6373-6378.
21. Onoda-Yamamuro, N., T. Matsuo, and H. Suga, Calorimetric and IR spectroscopic studies of phase transitions in methylammonium trihalogenplumbates (II). *Journal of Physical Chemistry of Solids*, 1990. **51**, 1383-1395.
22. Knop, O., R.E. Wasylishen, M.A. White, T.S. Cameron, and M.J.M. Van Voort, Alkylammonium lead halides. Part 2. CH3NH3PbX3 (X = C1, Br, I) perovskites: cuboctahedral halide cages with isotropic cation reorientation1. *Canadian Journal of Chemistry*, 1990. **68**, 412-422.
23. Zhang, H., X. Qiao, Y. Shen, T. Moehl, S.M. Zakeeruddin, M. Gratzel, and M. Wang, Photovoltaic behaviour of lead methylammonium triiodide perovskite solar cells down to 80 K. *Journal of Material Chemistry A*, 2015, DOI: 10.1039/c5ta02206a.
24. D'Innocenzo, V., G. Grancini, M.J.P. Alcocer, A.R.S. Kandada, S.D. Stranks, M.M. Lee, G. Lanzani, H.J. Snaith, and A. Petrozza, Excitons Versus Free Charges in Organo-Lead tri-Halide Perovskites. *Nature Communications*, 2014. **5**, 3586.
25. Mashiyama, H., Y. Kawamura, E. Magome, and Y. Kubota, Displacive character of the cubic-tetragonal transition in $CH_3NH_3PbIX_3$. *Journal of Korean Physical Society*, 2003. **42**, S1026-S1029.
26. Glazer, A.M., The classification of tilted octahedral in perovskites. *Acta Crystallographica*, 1972. **B28**, 3384-3392.
27. Baikie, T., Y. Fang, J.M. Kadro, M. Schreyer, F. Wei, S.G. Mhaisalkar, M. Graetzel, and T.J. Whitec, Synthesis and Crystal Chemistry of the Hybrid Perovskite $(CH_3NH_3)PbI_3$ for Solid-State Sensitised Solar Sell Applications. *J. Mater. Chem. A*, 2013. **1**, 5628–5641.
28. Weller, M.T., O.J. Weber, P.F. Henry, A. Di Pumpo, and T.C. Hansen, Complete structure and cation orientation in the perovskite photovoltaic methylammonium lead iodide between 100 and 352 K. *Chemical Communications*, 2015. **51**, 4180-4183.
29. Fang, H.-H., R. Raissa, M. Abdu-Aguye, S. Adjokatse, G.R. Blake, J. Even, and M.A. Loi, Photophysics of organic-inorganic hybrid lead iodide perovskite single crystals. *Advanced Functional Materials*, 2015. **25**, 2378-2385.
30. Ashcroft, N.W. and N.D. Mermin, *Solid State Physics*, ed. H.R. Winston1976: Holt Rinehart & Winston.
31. Frost, J.M., K.T. Butler, F. Brivio, C.H. Hendon, M.v. Schilfgaarde, and A. Walsh, Atomistic Origins of High-Performance in Hybrid Halide Perovskite Solar Cells. *Nano Letters*, 2014. **14**, 2584–2590.
32. Varshni, Y.P., Temperature dependence of the energy gap in semiconductors. *Physica*, 1967. **34**, 149-154.
33. Foley, B.J., D.L. Marlowe, K. Sun, W.A. Saidi, L. Scudiero, M.C. Gupta, and J.J. Choi, Temperature dependent energy levels of methylammonium lead iodide perovskite. *Applied Physical Letters*, 2015. **106**, 243904.
34. Tao, C., S. Neutzner, L. Colella, S. Marras, A.R.S. Kandada, M. Gandini, M. De Bastiani, G. Pace, L. Manna, M. Caironi, C. Bertarelli, and A. Petrozza, 17.6% stabilized efficiency in

Energy & Environmental Science Accepted Manuscript

low-temperature processed planar perovskite solar cells. *Energy and Environmental Science*, 2015. **8**, 2365-2370.

35. Giannozzi, P., S. Baroni, N. Bonini, M. Calandra, R. Car, C. Cavazzoni, D. Ceresoli, G.L. Chiarotti, M. Coccioni, I. Dabo, A. Dal Corso, S. de Gironcoli, S. Fabris, G. Fratesi, R. Gebauer, U. Gerstmann, C. Gougoussis, A. Kokalj, M. Lazzeri, L. Martin-Samos, N. Marzari, F. Mauri, R. Mazzarello, S. Paolini, A. Pasquarello, L. Paulatto, C. Sbraccia, S. Scandolo, G. Sclauzero, A.P. Seitsonen, A. Smogunov, P. Umari, and R.M. Wentzcovitch, QUANTUM ESPRESSO: a Modular and Open-Source Software Project for Quantum Simulations of Materials. *Journal of Physics: Condensed Matter*, 2009. **21**, 395502.
36. Umari, P., E. Mosconi, and F. De Angelis, Relativistic GW Calculations on $CH_3NH_3PbI_3$ and $CH_3NH_3SnI_3$ Perovskites for Solar Cell Applications. *Scientific Reports*, 2014. **4**, 4467/1-4.
37. Brivio, F., K.T. Butler, A. Walsh, and M. van Schilfgaarde, Relativistic Quasiparticle Self-Consistent Electronic Structure of Hybrid Halide Perovskite Photovoltaic Absorbers. *Physical Review B*, 2014. **89**, 155204/1-6.
38. Grancini, G., S. Marras, M. Prato, C. Giannini, C. Quarti, F. De Angelis, M. De Bastiani, G.E. Eperon, H.J. Snaith, L. Manna, and A. Petrozza, The impact of the crystallization processes on the structural and optical properties of hybrid perovskite films for photovoltaics. *Journal of Physical Chemistry Letters*, 2014. **5**, 3836-3842.
39. Yu, H., F. Wang, F. Xie, W. Li, J. Chen, and N. Zhao, The role of chlorine in the formation process of "CH3NH3PbI$_{3-x}$Cl$_x$ perovskite. *Advanced Functional Materials*, 2014. **24**, 7102-7108.
40. Colella, S., E. Mosconi, P. Fedeli, A. Listorti, F. Gazza, F. Orlandi, P. Ferro, T. Besagni, A. Rizzo, G. Calestani, G. Gigli, F. De Angelis, and R. Mosca, $MAPbI_{3-x}Cl_x$ Mixed Halide Perovskite for Hybrid Solar Cells: The Role of Chloride as Dopant on the Transport and Structural Properties. *Chemistry of Materials*, 2013. **25**, 4613–4618.
41. Colella, S., E. Mosconi, G. Pellegrino, A. Alberti, V.L.P. Guerra, S. Masi, A. Listorti, A. Rizzo, G.G. Condorelli, F. De Angelis, and G. Gigli, Elusive presence of chlorine in mixed halide perovskite solar cells. *Journal of Physical Chemistry Letters*, 2014. **5**, 3532-3538.
42. Mosconi, E., A. Amat, M.K. Nazeeruddin, M. Graetzel, and F. De Angelis, First-Principles Modeling of Mixed Halide Organometal Perovskites for Photovoltaic Applications. *Journal of Physical Chemistry C*, 2013. **117**, 13902−13913.
43. Quarti, C., E. Mosconi, and F. De Angelis, Interplay of Orientational Order and Electronic Structure in Methylammonium Lead Iodide: Implications for Solar Cells Operation. *Chemistry of Materials*, 2014. **26**, 6557–6569.
44. Kawamura, Y., H. Mashiyama, and K. Hasebe, Structural study on cubic-tetragonal transition of $CH_3NH_3PbI_3$. *Journal of Physical Society of Japan*, 2002. **71**, 1694-1697.
45. Mashiyama, H., Y. Kurihara, and T. Azetsu, Disordered cubic perovskite structure of $CH_3NH_3PbX_3$ (X=Cl, Br, I). *Journal of Korean Physical Society*, 1998. **32**, S156-S158.
46. Worhatch, R.J., H.J. Kim, I.P. Swainson, A.L. Yonkeu, and S.J.L. Billinge, Study of local structure in selected organic-inorganic perovskite in the Pm3m phase. *Chemistry of Materials*, 2008. **20**, 1272-1277.
47. Maalej, A., Y. Abid, A. Kallel, A. Daoud, A. Lautié, and F. Romain, Phase transitions and crystal dynamics in the cubic perovskite $CH_3NH_3PbCl_3$. *Solid State Communications*, 1997. **103**.
48. Wasylishen, R.E., O. Knop, and J.B. Macdonald, Cation rotation in methylammonium lead halides. *Solid State Communications*, 1985. **56**, 581-582.
49. Car , R. and M. Parrinello, Unified Approach for Molecular Dynamics and Density-Functional Theory. *Physical Review Letters*, 1985. **55**, 2471–2474.

Energy & Environmental Science Accepted Manuscript

50. Quarti, C., E. Mosconi, and F. De Angelis, Structural and electronic properties of organo-halide hybrid perovskites from ab initio molecular dynamics. *Physical Chemistry Chemical Physics*, 2015. **17**, 9394-9409.
51. Choi, J.J., X. Yang, Z.M. Norman, S.J.L. Billinge, and J.S. Owen, Structure of Methylammonium Lead Iodide Within Mesoporous Titanium Dioxide: Active Material in High-Performance Perovskite Solar Cells. *Nano Letters*, 2013. **14**, 127-133.
52. Even, J., L. Pedesseau, J.-M. Jancu, and C. Katan, Importance of Spin−Orbit Coupling in Hybrid Organic/Inorganic Perovskites for Photovoltaic Applications. *Journal of Physical Chemistry Letters*, 2013. **4**, 2999-3005.
53. Amat, A., E. Mosconi, E. Ronca, C. Quarti, P. Umari, M.K. Nazeeruddin, M. Grätzel, and F. De Angelis, Cation-Induced Band-Gap Tuning in Organohalide Perovskites: Interplay of Spin–Orbit Coupling and Octahedra Tilting. *Nano Letters*, 2014.
54. Yuan, Y., X. Zhengguo, B. Yang, and J. Huang, Arising applications of ferroelectric materials in photovoltaic devices. *Journal of Material Chemistry A*, 2013. **2**, 6027-6041.
55. Liu, S., F. Zheng, N.Z. Koocher, H. Takenaka, F. Wang, and A.M. Rappe, Ferroelectric domain wall induced band gap reduction and charge separation in organometal halide perovskites. *Journal of Physical Chemistry Letters*, 2'014. **6**, 693-699.
56. Stroppa, A., C. Quarti, F. De Angelis, and S. Picozzi, Ferroelectric polarization of CH3NH3PbI3: a detailed study based on density functional theory and symmetry mode analysis. *Journal of Physical Chemistry Letters*, 2015. **6**, 2223-2231.
57. Beilstein-Edmands, J., G.E. Eperon, M.B. Johnston, H.J. Snaith, and P.G. Radaelli, Non-ferroelectric nature of the conductance hysteresis in $CH_3NH_3PbI_3$ perovskite-based photovoltaic devices. 2015.
58. Ma, J. and L.W. Wang, Nanoscale charge localization induced by random orientations of organic molecules in hybrid perovskite $CH_3NH_3PbI_3$. *Nano Letters*, 2015. **15**, 248-253.
59. Dymshits, A., A. Henning, G. Segev, Y. Rosenwaks, and E. L., The electronic structure of metal oxide/organo metal halide perovskite junctions in perovskite based solar cells. *Nature*, 2014. **5**, 8704/1-6.

Energy & Environmental Science Accepted Manuscript